

# Edge-cracked Plates with Centric Hole Subject to Fluctuated Loads and Ambient Heat

Hsin-Yi Lai\* and Xuan-Wei Liu\*

**Keywords:** *thermoelastic and fracture properties, stress intensity factor, meshfree RPIM*

## ABSTRACT

This paper aims to characterize the thermo-elastic and fracture properties of an edge-cracked plate with centric hole subject to ambient heat and fluctuated loads. A Radial Point Interpolation Meshless (RPIM) method is first developed and used to estimate the associated stress intensity factor (SIF) for such a complicated problem. It is found that the solution thus obtained by RPIM is somehow more precise than that obtained by the FEM. The influence of edge-cracked locations and lengths on the displacement of the plate that bears fluctuated loads and ambient heat are carefully characterized and presented. Simulation results also reveal that both thermoelastic and fracture properties of the edge-cracked plate with centric hole can be more efficiently and accurately modeled by using the proposed RPIM approach.

## INTRODUCTION

With fast advancement in structural technology, the exploration on edge-cracked plates with centric holes have emerged as a research area interested to many aerospace engineers in the past several decades [Tanigawa, 1995]. The concept in dealing with structural and thermal barriers problems encountered in space planes are mainly used at various ambient temperature environment, including thermal shock or being heated/cooled in short time. The discontinuous interface of the edge-cracked plate with centric hole is very likely to cause stress intensity in different severe environment.

In case that there exists cracks or vacancies in the structure, it can largely reduce the strength and life of the structure. Since in many hardship environment it is inevitable that there exist some unexpected material defects, vacancies and cracks inside structures and it is

also very difficult to get effective analytical solutions for solving such improper inhomogeneous structures with cracks and complicated boundary conditions, it is thus desperately needed to come up with some methods to effectively predict the dynamic behaviours of such structures in various severe environments.

In order to circumvent the problems, this paper proposes a RPIM method intended to characterize the thermoelastic and fracture properties of edge-cracked plates made of steel subject to high ambient heat and fluctuating loads.

Meshfree methods have been developed for over two decades. There are several different computational schemes that have been proposed in the literature including smooth particle hydrodynamics (SPH; Gingold and Monaghan, 1977), diffuse element method (DEM; Nayroles, Touzot and Villon, 1992), element free Galerkin method (EFGM; Belytschko, Lu and Gu, 1994), meshfree local Petrov-Galerkin method (MLPG; Atluri and Zhu, 1998), point interpolation method (PIM; Atluri and Zhu, 2001) and radial point interpolation method (RPIM; Liu, Zhang, Gu and Wang, 2005), and so on. The main concept of meshfree method is to establish a system of algebraic governing equations without using a predefined mesh for domain discretization. Meshfree methods use arbitrary and scattered nodes that have no relationship among them to discrete governing equations. There are several methods that have been applied to structural analysis. The approach of RPIM selected for this study is a radial basis functional approximation that satisfies Kronecker's delta properties. The method is easy to enforce essential boundary conditions and inclusion of direct method and penalty functions.

With such an efficient method, the characterization of thermo-elastic and fracture properties for edge-cracked plates made of steel subject to ambient heat and fluctuates loads is made possible. The influence of crack locations and volume fractions on stress intensity factor and the displacement of the steel plate were elaborated in details in the context.

## METHODOLOGY

Meshless methods were originally proposed by Slater [1934] and Barta [1937] using collocation methods and by Chorin [1973] using vortex methods. The SPH

*Paper Received January, 2019. Revised March, 2019. Accepted April, 2019. Author for Correspondence: Hsin-Yi Lai.*

*\* Department of Mechanical Engineering, National Cheng Kung University, Tainan, Taiwan, ROC.*

(Smoothed Particle Hydrodynamics) method were proposed by Lucy [1977], and Gingold and Monaghan [1077] to solve for three-dimensional astrophysics problem in outer space initially and many others astrophysics applications later on. In this paper, The modeling procedures for using the RPIM for analyzing problems of cracked plates are given below as (1) to represent the domain problem by a group of randomly distributed particles that have no connection and no grid, and then construct shape functions by using the procedures of RPIM, (2) to form particle field functions in support domain based upon constructed shape functions, and convert system governing equations into integral expression in its weak form, (3) to apply particle field functions to system differential equations, replace system integral expression by background grids, represent each node function in problem domain in terms of global stiffness and mass matrices, and finally, compute the values of particle field functions, (4) to follow the same procedures given above to formulate system RPIM to solve cracked plate problems subject to ambient thermal loads, (5) to construct material properties for plate made of steel, and (6) to formulate and solve the edge-cracked plate problems subject to both fluctuated and ambient thermal loads.

### Constructing RBFs and Shape Functions

First of all, the radial basis functions (RBFs) are employed to avoid domain singularity and to develop the RPIM shape functions for meshfree weak-form. The RBFs are given as

$$u(x) = \sum_{i=1}^n R_i(x) a_i + \sum_{j=1}^m p_j(x) b_j = R^T(x) a + p^T(x) b \quad (1)$$

where  $R(x)$  is the radial basis function,  $p_j(x)$  is the monomial in  $x$  and  $y$  coordinates,  $n$  is the number of radial basis functions,  $R(x)$  is the function of distance  $r$ , between the point of interest  $x$  and any arbitrary node at  $x_i$  that is given as

$$r = \sqrt{(x - x_i)^2 + (y - y_i)^2} \quad (2)$$

Many different types of radial basis functions and the characteristics of RBFs have been widely discussed in the literature including multi-quadrics (MQs), Gaussian exponential functions, thin plate spline (TPS) and logarithmic radial basis functions. In this work, MQs are used to develop shape functions. Here, MQs are given as

$$R_i(x, y) = \left( r_i^2 + (\alpha_c d_c)^2 \right)^q \quad (3)$$

where  $d_c$  is the characteristic length, often chosen as the average distance among nodes in system domain,  $\alpha_c$  and  $q$  are parameters to be determined for the performance.

In order to solve for unknown coefficients of vectors  $a$  and  $b$  in Eq. (1), the system is forced to be satisfied at  $n$  specific nodes surrounding the point of interest  $x$ . That will lead to  $n$  different equations that can be expressed as

$$U_s = R_0 a + P_m b \quad (4)$$

where the vector expression of  $U_s$  is given as

$$U_s = \{u_1 \quad u_2 \quad \dots \quad u_n\}^T \quad (5)$$

$R_0$ , the moment matrix of RBFs, is in its expression as

$$R_0 = \begin{bmatrix} R_1(r_1) & R_2(r_1) & \dots & R_n(r_1) \\ R_1(r_2) & R_2(r_2) & \dots & R_n(r_2) \\ \vdots & \vdots & \ddots & \vdots \\ R_1(r_n) & R_2(r_n) & \dots & R_n(r_n) \end{bmatrix} \quad (6)$$

$r_k$ , distance between the point of interest  $x_k$  and any arbitrary node at  $x_i$ , is defined by

$$r_k = \sqrt{(x_k - x_i)^2 + (y_k - y_i)^2} \quad (7)$$

and  $p_m^T$ , the polynomial moment matrix, is given as

$$P_m^T = \begin{bmatrix} 1 & 1 & \dots & 1 \\ x_1 & x_2 & \dots & x_n \\ y_1 & y_2 & \dots & y_n \\ \vdots & \vdots & \ddots & \vdots \\ p_m(x_1) & p_m(x_2) & \dots & p_m(x_n) \end{bmatrix} \quad (8)$$

Since there are  $n+m$  variables in Eq. (8), one needs to add another  $m$  equations to solve the problem. By assuming

$$P_m^T a = \sum_{i=1}^n p_j(x_i) a_i = 0 \quad (9)$$

and plugging Eq. (9) into Eq. (4), one can obtain

$$\tilde{U}_s = \begin{bmatrix} U_s \\ 0 \end{bmatrix} = \begin{bmatrix} R_0 & P_m \\ P_m^T & 0 \end{bmatrix} \begin{bmatrix} a \\ b \end{bmatrix} = G a_0 \quad (10)$$

Since  $R_0$  is a symmetric matrix, matrix  $G$  will thus be symmetric as well. By solving for the inverse form of  $G$ , one can easily obtain

$$a_0 = \begin{Bmatrix} a \\ b \end{Bmatrix} = G^{-1} \tilde{U}_s \quad (11)$$

Now, by plugging Eq. (11) into Eq. (1), the RBFs can be obtained as

$$u(x) = R^T(x) a + p^T(x) b = \{R^T(x) \quad p^T(x)\} G^{-1} \tilde{U}_s \quad (12)$$

Finally, by rearranging the above equation, one has

$$u(x) = R^T(x) a + p^T(x) b = \{R^T(x) \quad p^T(x)\} G^{-1} \tilde{U}_s = \tilde{\Phi}^T(x) \tilde{U}_s \quad (13)$$

where the shape function,  $\tilde{\Phi}^T(x)$ , can be expressed as

$$\tilde{\Phi}^T(x) = \{\phi_1(x) \quad \phi_2(x) \quad \dots \quad \phi_n(x) \quad \phi_{n+1}(x) \quad \dots \quad \phi_{n+m}(x)\} \quad (14)$$

### Formulating Global Galerkin Weak-form

Global Galerkin weak-form can be derived by using Galerkin weighted residual method, virtual work principle and the principle of minimum potential energy. As known, engineering problems are governed by ODEs/PDEs along with sets of initial/boundary conditions. Consider the system governing equation in problem domain  $\Omega$  being realized as

$$A(u) + b = 0 \quad (15)$$

where  $A$  is a differential operator expressed in terms of the scalar function  $u$ , and the condition on boundary  $\Gamma$  is given as

$$C(u) = d \quad (16)$$

where  $C$  is a differential operator associated with boundary  $\Gamma$ , and  $u$  can be approximated by

$$u^p = \sum_{i=1}^n \alpha_i B_i(x) \quad (17)$$

where  $B_i(x)$  are basis functions,  $a_i$  are unknown coefficients of basis functions, and  $n$  is the number of basis functions. By plugging Eq. (17) into Eqs. (15~16), one can obtain

$$A(u^p) + b \neq 0 \quad (18)$$

$$C(u^p) - d \neq 0 \quad (19)$$

The associated residual functions of  $R_A$  and  $R_C$  can be estimated, respectively, by

$$R_A = A(u^p) + b \quad (20)$$

$$R_C = C(u^p) - d \quad (21)$$

Note that  $R_A$  and  $R_C$  are both varied with approximate functions used. In order to minimize the overall residuals, the weighted integrals of residual functions are being forced to zero. That should lead to

$$\int_{\Omega} W_i R_A d\Omega + \int_{\Gamma} Q_i R_C d\Gamma = 0 \quad (22)$$

where  $W_i$  and  $Q_i$  are the weighted functions of  $R_A$  and  $R_C$ . Equation (22) is the general form of overall weighted residuals that leads to a set of integral equations derived from original system differential equations of the form

$$L^T \sigma + b = \rho \ddot{u} + c \dot{u} \quad (23)$$

where  $\rho$  is the mass density,  $c$  is the damping coefficient,  $u$  is the displacement vector, and  $L$  is differential operator. The associated boundary condition are given as

$$\sigma_n = \bar{t} \quad \text{on the natural boundary} \quad (24)$$

$$u = \bar{u} \quad \text{on the essential boundary} \quad (25)$$

where the traction  $\bar{t}$  and displacements  $\bar{u}$  are of specific known values. Equation (23) can then be converted to the associated weak form given as

$$\int_{\Omega} (L\delta u)^T (DLu) d\Omega - \int_{\Omega} \delta u^T b d\Omega - \int_{\Gamma} \delta u^T (\rho \ddot{u} + c \dot{u}) d\Omega \quad (26)$$

where  $D$  is the stiffness matrix, and the associated approximate functions can now be expressed as

$$\delta u = \sum_I \phi_I u_I \quad (27)$$

$$L\delta u = \sum_I B_I \delta u_I \quad (28)$$

$$Lu = \begin{bmatrix} \frac{\partial \phi_1}{\partial x} & 0 & \dots & \frac{\partial \phi_n}{\partial x} & 0 \\ 0 & \frac{\partial \phi_1}{\partial y} & \dots & 0 & \frac{\partial \phi_n}{\partial y} \\ \frac{\partial \phi_1}{\partial y} & \frac{\partial \phi_1}{\partial x} & \dots & \frac{\partial \phi_n}{\partial y} & \frac{\partial \phi_n}{\partial x} \end{bmatrix} \begin{Bmatrix} u_1 \\ v_1 \\ \vdots \\ u_n \\ v_n \end{Bmatrix} = \sum_I B_I u_I \quad (29)$$

where  $\phi_i$  is the  $i$ -th shape function in the support domain. By plugging Eqs. (27~29) into Eq. (26), the approximate solution can now be given as

$$\int_{\Omega} (L\delta u)^T (DLu) d\Omega = \int_{\Omega} \sum_I \sum_J \delta u_I [B_I^T DB_J] u_J d\Omega \quad (30)$$

$$\text{where } B = \begin{bmatrix} \frac{\partial \Phi_i}{\partial x} & 0 & \frac{\partial \Phi_i}{\partial y} \\ 0 & \frac{\partial \Phi_i}{\partial y} & \frac{\partial \Phi_i}{\partial x} \end{bmatrix}^T \quad (31)$$

### Formulating Discretized System Equations

By expressing system equations in terms of discretized form of matrices, one has

$$M\ddot{U} + CU + KU = F^b + F^t \quad (32)$$

where  $M_{ij}$ , the mass matrix, is given as

$$M_{ij} = \int_{\Omega} \rho \phi_i^T \phi_j^T d\Omega \quad (33)$$

$K_{ij}$ , the stiffness matrix, is expressed as

$$K_{ij} = \int_{\Omega} [B_i^T DB_j] d\Omega \quad (34)$$

$C_{ij}$ , the damping matrix, is in its form as

$$C_{ij} = \int_{\Omega} c \phi_i^T \phi_j^T d\Omega \quad (35)$$

and  $F_i^b$  and  $F_i^t$ , the force matrices, are given as

$$F_i^b = \int_{\Gamma} \phi_i^T b d\Gamma \quad (36)$$

$$F_i^t = \int_{\Gamma} \phi_i^T \bar{t} d\Gamma \quad (37)$$

### RPIM Formulation for Thermal Loads

Consider a standard two-dimensional elastic problem in problem domain of  $\Omega$  with given boundary of  $\Gamma$ , and subjected to body force  $b$ . The governing equation can be expressed as

$$\rho c \frac{\partial T(x, y, t)}{\partial t} = \frac{\partial}{\partial x} (k_x \frac{\partial T(x, y, t)}{\partial x}) + \frac{\partial}{\partial y} (k_y \frac{\partial T(x, y, t)}{\partial y}) + Q \quad (38)$$

where  $\rho$  is the density of material,  $c$  is the specific heat,  $T(x, y, t)$  is temperature field,  $k_x$  and  $k_y$  are thermal conductivities in  $x$  and  $y$  directions, respectively, and  $Q$  is heat generation per unit volume. Also, the associated boundary and initial conditions are given as

$$T = \bar{T} \quad \text{on the essential boundary} \quad (39)$$

$$-k(\nabla T \cdot n) = \bar{q} \quad \text{on the natural boundary} \quad (40)$$

$$-k\nabla T \cdot n = h(T - T_{\infty}) \quad \text{on natural boundary} \quad (41)$$

$$T(x, y, 0) = T_0(x, y, 0) \quad \text{initial condition} \quad (42)$$

where  $\bar{q}$  is the heat flux,  $T_{\infty}$  is the temperature of environment,  $T_0(x, y, 0)$  and  $\bar{T}$  are of prescribed values.

By using the same procedures given above for elastic dynamic problems, the approximation solutions for temperature field can be expressed as

$$T^h(x, y, t) = \sum_{i=1}^n \phi_i^T(x, y) T(x, y, t) \quad (43)$$

By plugging Eq. (41) into system governing equation (38), the associated weak form can then be derived to obtain

$$C\dot{T} + KT = F(T, t) \quad (44)$$

where the elements of  $C$ ,  $K$  and  $F$  matrices are given as

$$C_{ij} = \int_{\Omega} \rho c \phi_i \phi_j d\Omega \quad (45)$$

$$K_{ij} = \int_{\Omega} k_x \left[ \frac{\partial \phi_i}{\partial x} \frac{\partial \phi_j}{\partial x} \right] + k_y \left[ \frac{\partial \phi_i}{\partial y} \frac{\partial \phi_j}{\partial y} \right] d\Omega + \int_{\Gamma_1} h \phi_i \phi_j d\Gamma \quad (46)$$

$$F_i = \int_{\Omega} Q \phi_i d\Omega - \int_{\Gamma_1} \bar{q} \phi_i d\Gamma - \int_{\Gamma_1} h T_{\infty} \phi_i d\Gamma \quad (47)$$

**Edge-cracked Plate Subject to Ambient Heat**

Since the paper aims to characterize thermodynamic behaviors of the edge-cracked steel plate by using RPIM, elastic deformation of the plate subject to ambient heat and fluctuated loads is thus presumed for physical realization purpose. Here, we are not concerned with the problem of crack propagation subject to long-term external loading effect. Only the variation of the stress-strain relation and thermal distribution of the edge-cracked plate associated with thermo-elastic and fracture properties of the plate are concerned for further exploration.

Consider the transient heat conduction problem of a 2D plate. The system governing equation and associated boundary conditions are given as

$$\rho c \frac{\partial T(x, y, t)}{\partial t} = \frac{\partial}{\partial x} \left( k_x \frac{\partial T(x, y, t)}{\partial x} \right) + \frac{\partial}{\partial y} \left( k_y \frac{\partial T(x, y, t)}{\partial y} \right) + Q \quad (48)$$

Specific b.c.'s  $T = \bar{T}$  along  $\Gamma_0$  (49)

Natural b.c.'s  $-k(\nabla T \cdot n) = \bar{q}$  along  $\Gamma_1$  (50)

$$-k \nabla T \cdot n = h(T - T_{\infty}) \text{ along } \Gamma_2 \quad (51)$$

i.c.  $T(x, y, 0) = T_0(x, y, 0)$  along  $\Omega$  (52)

where  $\rho$  is the density,  $c$  is specific heat,  $T(x, y, t)$  is temperature distribution of the plate,  $k_x$  and  $k_y$  are heat conductivities along  $x$  and  $y$  directions, respectively,  $h$  is the convective coefficient,  $T_{\infty}$  is ambient temperature, and  $Q$  is of the heat source. Thus, the distribution of field temperature is given as

$$T^h(x, y, t) = \sum_{i=1}^N \phi_i^T(x, y) T(x, y, t) \quad (53)$$

By plugging Eq. (53) into the weak form of Eq. (48), one can now obtain

$$C\dot{T} + KT = F(T, t) \quad (54)$$

where

$$C_{ij} = \int_{\Omega} \rho c \phi_i \phi_j d\Omega \quad (55)$$

$$K_{ij} = \int_{\Omega} k_x \left[ \frac{\partial \phi_i}{\partial x} \frac{\partial \phi_j}{\partial x} \right] + k_y \left[ \frac{\partial \phi_i}{\partial y} \frac{\partial \phi_j}{\partial y} \right] d\Omega + \int_{\Gamma_1} h \phi_i \phi_j d\Gamma \quad (56)$$

$$F_i = \int_{\Omega} Q \phi_i d\Omega - \int_{\Gamma_1} \bar{q} \phi_i d\Gamma - \int_{\Gamma_1} h T_{\infty} \phi_i d\Gamma \quad (57)$$

**Time integration of transient terms**

Once strong form expressions were converted into weak forms, time transient terms are required to be dealt with immediately. Here, Crank-Nicholson scheme [1947] is employed to integrate the differentiators associated with transient terms, and accordingly, Eqs. (55-57) can be discretized easily to have

$$\tilde{K}_{s+1} T_{s+1} = \tilde{K}_s T_s + \tilde{F} \quad (58)$$

where

$$\tilde{K}_{s+1} = C_{s+1} + \frac{1}{2} \delta t_{s+1} K_{s+1} \quad (59)$$

$$\tilde{K}_s = C_s - \frac{1}{2} \delta t_{s+1} K_s \quad (60)$$

$$\tilde{F} = \frac{1}{2} \delta t_{s+1} (F_s + F_{s+1}) \quad (61)$$

**Boundary and working conditions near cracks**

Several basic assumptions are made to allow the investigation of the edge-cracked plate and the plate with a centric hole subject to ambient heat and fluctuated loads more precise. These assumptions include:

1. The crack length and location on the plate are specified beforehand. The crack length is specified initially and the crack width is ignored.
2. Thermo-elastic properties of the cracks and modes of heat exchange including conduction, convection and radiation among cracks are assumed negligible.
3. Boundaries near cracks are assumed to be visible. In other words, in process of estimating shape functions, both the defined and influence domains are assumed mutually isolated to each other and thus no overlapping effect will occur.

**Stress intensity factor (SIF) for a cracked plate**

The stress intensity factor (SIF) for a edge-cracked plate subject to fluctuated loads and ambient heat is estimated by using both the RPIM and FEM. It is then compared with the analytical solution to estimate the accuracy of these two different approaches. The analytical solution of SIF for a cracked plate [Gladwell, 1996] is given as

$$K_I = \sigma \sqrt{a} \left[ 1.12\sqrt{\pi} - 0.41 \frac{a}{W} + 18.7 \left( \frac{a}{W} \right)^2 - 38.48 \left( \frac{a}{W} \right)^3 + 53.85 \left( \frac{a}{W} \right)^4 \right] \quad (62)$$

where  $K_I$  is the SIF for the crack of mode  $I$ ,  $w$  is the width of the plate,  $a$  is the length of the crack.

Also, the analytical solution of stress  $\sigma_{\theta\theta}(r)$  at a point of distant  $r$  in radial direction [15] for a plate with centric hole of radius  $a$  as subjected to lateral loads, is given as

$$\sigma_{\theta\theta}(r) = \sigma \left[ 1 + 0.5 \left( \frac{a}{r} \right)^2 + 1.5 \left( \frac{a}{r} \right)^4 \right] \quad (63)$$

**RESULTS AND DISCUSSION**

In order to verify the accuracy and efficiency of the proposed RPIM, an edge-cracked steel plate and a steel plate with centric hole subject to lateral fluctuated loads are employed for modeling using both RPIM and FEM, in an attempt to compare with analytic solutions. In this comparative study, the parameter of the influence domain is set to 3, and radian interpolation coefficients are given for  $q = 1.03$ , and  $a_c d_c = 1$ .

**RPIM and FEM modeling of edge-cracked steel plate subject to lateral fluctuated loads**

Figure 1 shows the dimensions of edge-cracked steel plate subject to lateral fluctuated loads of  $f(t) = 1000 \cdot \sin(t)$  MPa along both vertical edges in y-direction. The geometric sizes and material properties of the edge-cracked steel plate are given in Table 1. Figure 2 shows the x-displacement of edge-cracked steel plate subject to lateral fluctuated loads of  $f(t) = 1000 \cdot \sin(t)$  MPa on both vertical edges in y-direction. Table 2 shows the x-displacements obtained by the proposed RPIM using  $25 \cdot 13$  nodal points and traditional FEM using 27450 nodal points with 4950 elements. As compared to analytic solution given by Eq. (60), the error obtained by RPIM is merely 1.15%, and -22.5% for that obtained by FEM approach.

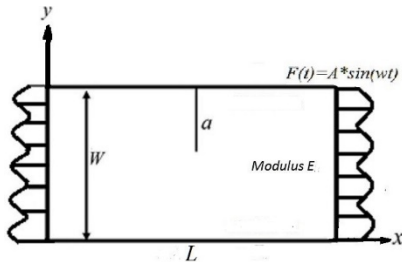


Fig. 1 Edge-cracked plate subject to fluctuated lateral loads of  $1000 \cdot \sin(t)$  MPa

Table 1 Dimensions, material properties and working conditions of the edge-cracked steel plate

sizes of the plate	$L=24$ mm $W=12$ mm
crack length $a$	$a = 6$ mm
fluctuated loads	$F(t)=1000 \cdot \sin(t)$ MPa
density	$7850$ kg/m <sup>3</sup>
Young's modulus	$200$ GPa
Poisson ratio	$0.3$

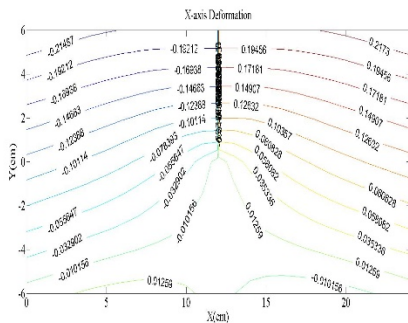


Fig. 2 Displacement of edge-cracked plate subject to lateral fluctuated loads of  $1000 \cdot \sin(t)$  MPa

Table 2 Plate stresses and SIFs at (12 mm, 7 mm) by using RPIM, FEM and analytic approach

approaches	Analytics	RPIM	FEM
nodes used	--	$25 \cdot 13$	27456
stress (Mpa)	4896	4954	3795
stress intensity factor	12273	12415	9510
error (%)	--	1.15	-22.5

**RPIM and FEM modeling of steel plates with centric hole subject to lateral fluctuated loads**

Figure 3 shows the sizes of steel plate with a centric hole subject to lateral fluctuated loads of  $f(t) =$

$1000 \cdot \sin(t)$  MPa along vertical edges. The geometric sizes and material properties of the edge-cracked steel plate are given in Table 3. Figure 4 shows the stresses of  $S_{yy}$  at two arbitrarily chosen radial points of  $r=4$  mm and  $r=5$  mm measured from the hole center of the steel plate by using RPIM, FEM and analytic solution of Eq. (63).

As shown in Fig. 4, it is obvious that the stress intensity factor (SIF) reaches its maximum of 3 at  $r = a = 3$  mm, and decreases as the radial distance  $r$  increases. The modeling error of SIF for the aforementioned case is approximately 30% for using RPIM and 45% for using FEM at  $r = 4$  mm. The percentage error of both RPIM and FEM modeling decreases as the measured distance  $r$  from the hole center increases. The error percentage is thus gradually reduced to 6.7% for RPIM at  $r = 6$  mm.

In case the geometry of the crack and centric hole becomes irregular, the modeling errors can possibly increase largely due to improper selection of locations and numbers of nodal points in the given problem domain. Therefore, for problems of irregular cracks and holes in the structure, the selection of proper locations and numbers of nodal points is very crucial since that can significantly affect the modeling results, especially for problems with limited numbers of nodal points in numerical modeling process of RPIM, as given in Fig. 5.

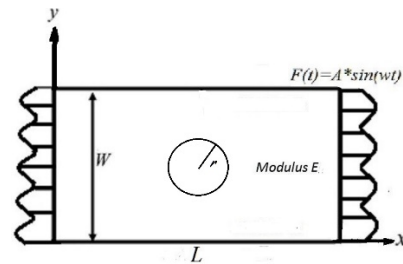


Fig. 3 Steel plate with a centric hole subject to fluctuated lateral loads of  $1000 \cdot \sin(t)$  MPa

Table 3 Dimensions, material properties and working conditions of the steel plate with a centric hole

sizes of the plate	$L=24$ mm $W=12$ mm
radius of centric hole	$r = 3$ mm
fluctuated loads	$F(t)=1000 \cdot \sin(t)$ MPa
density	$7850$ kg/m <sup>3</sup>
Young's modulus	$200$ GPa
Poisson ratio	$0.3$

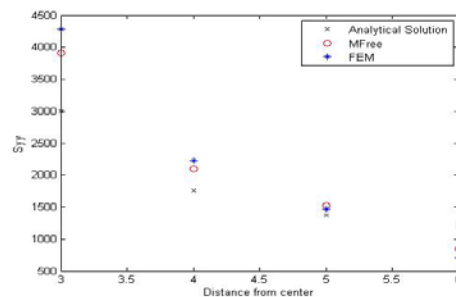


Fig. 4 Plate stresses  $S_{yy}$  at two given radial points of  $r=4$  mm and  $r=5$  mm measured from the hole center of the steel plate by using RPIM, FEM and analytic approaches

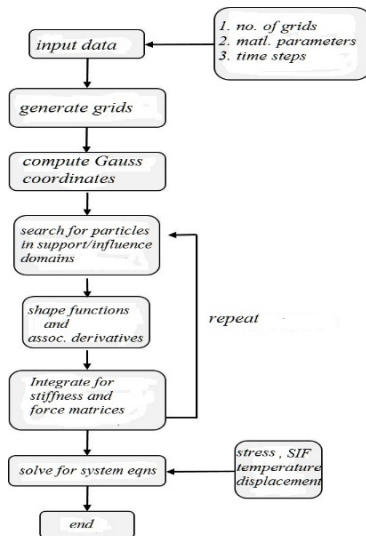


Fig. 5 Nodal selection and RPIM modeling process

**Edge-cracked steel plate subject to ambient heat**

Figure 6 shows the edge-cracked steel plate subject to ambient thermal loads on the right-hand side with temperature of 10°C. The geometric sizes and material properties of the plate are given in Table 4. The temperature distribution of the edge-cracked steel plate is given in Figure 7(a) and (b) at time steps of 5000 and 10000, respectively. It is obvious that the edge-crack on the steel plate acting as an adiabatic barrier that prevents the heat on the right-hand side of the crack from passing through the gap, and thus enforce the heat to detour and retard the heat propagation leading to a longer conduction time.

Table 5 shows the temperature differences of the retard time of the heat propagation of the edge-cracked plate as compared to those obtained from the flat steel plate without crack. The temperature differences are measured at three arbitrarily chosen points, namely, (-1.2 mm, 1.2mm), (0 mm, -1.2 mm), and (1.2 mm, 1.2 mm), and modeling by RPIM using 21\*11 nodal points and FEM using 47760 nodal points with 9225 elements. Table 5 indicates that as time passes the temperature at point (1.2 mm, 1.2 mm) is always higher than the temperature at point (0 mm, -1.2 mm), and the temperature at point (-1.2 mm, 1.2mm) on the left-hand bank of the crack gap is always of the lowest one among these three selected points.

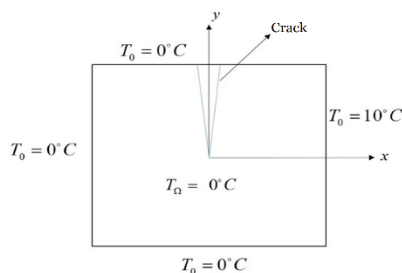


Fig. 6 Edge-cracked squared plate made of steel as subjected to lateral thermal load on r.h.s.

Table 4 Dimensions, material properties and working conditions of edge-cracked squared steel plate

sizes of the plate	L=12 mm W=12 mm
crack length	a = 6 mm
ambient temperature	10°C on r.h.s
time step for RPIM & FEM	0.008 s
density	7850 kg/m <sup>3</sup>
specific heat	434 J/Kg-C
thermal conductivity	60.4 W/m-K

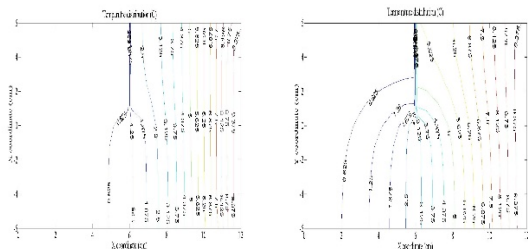


Fig. 7 Plate temperature obtained by RPIM at time steps of (a) 5000 and (b) 10000

Table 5 Temperature distribution at three randomly chosen nodes for edge-cracked squared steel plate subject to lateral thermal load of T=10°C on r.h.s.

time (s)	method	(-1.2 cm, 1.2 cm)	(0 cm, -1.2 cm)	(1.2 cm, 1.2 cm)
40	FEM	0.181	1.121	2.409
	RPIM	0.256	1.194	2.493
56	FEM	0.402	1.795	3.477
	RPIM	0.528	1.875	3.531
72	FEM	0.642	2.365	4.317
	RPIM	0.808	2.443	4.334
88	FEM	0.875	2.836	4.973
	RPIM	1.071	2.910	4.958

**Steel plates with centric hole subject to ambient thermal loads**

Figure 8 shows the steel plate with a centric hole subject to ambient heat of temperature of 100 °C on upper boundary, 100°C on other boundaries and 500 °C around the centric hole. The geometric sizes, material properties and working conditions of the plate are given in Table 5. The simulation was carried out using RPIM for 500 time steps with 0.05 second per step.

Figure 9 shows the temperature distribution of the steel plate with a centric hole subject to T=100 °C on the upper boundary, T=50 °C on other plate boundaries and T=500 °C around the centric hole. It is obvious that the temperature contours are somewhat symmetric along horizontal x-direction, and become denser with higher temperature gradient in positive y-direction.

Figure 10 shows nodal positions of the steel plate subject to the same thermal loads as above. The result indicates that the displacements for nodes of higher temperature gradient are subject to tensile stress in positive y-direction, and the displacements for nodes of symmetric contour are subsequently subject to compressive stress along the horizontal x-direction. Thus, the temperature induced displacement phenomenon becomes distinct around centric hole areas.

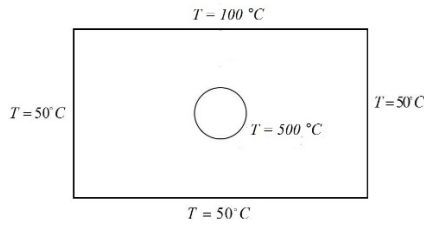


Fig. 8 Schematic diagram for the steel plate with a centric hole as subjected to ambient thermal loads

Table 6 Dimensions, material properties, and working conditions of the steel plate with a centric hole

sizes of the plate	L=24 cm W=11 cm
radius of centric hole	2.5 cm
ambient temperature	100°C on top boundary 500°C around centric hole 50°C on other boundaries
time step for RPIM & FEM	0.05 sec
density	7850 kg/m <sup>3</sup>
specific heat	434 J/Kg-C
thermal conductivity	60.4 W/m-K

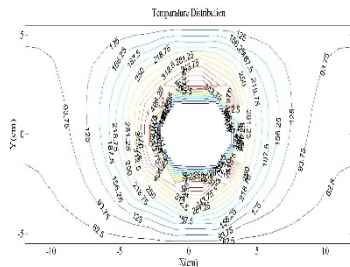


Fig. 9 Temperature distribution of the steel plate with a centric hole as subjected to T=100°C on upper boundary, T=500°C around centric hole, and T=50°C on all other boundaries

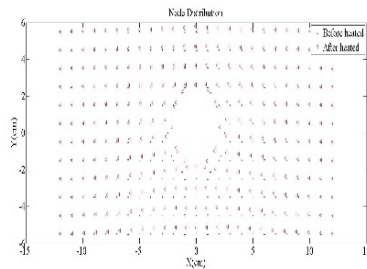


Fig. 10 Nodal positions before and after thermal loadings for the steel plate with a centric hole subject to T=100°C on upper boundary, T=500°C around centric hole, and T=50°C on all other boundaries

## CONCLUSIONS

Since it is difficult to obtain exact solutions for edge-cracked plate subject to ambient heat and fluctuated loads, this paper presents the meshless RPIM to characterize the associated thermoelastic and fracture properties. Giving the procedures and simulations presented above, several conclusions can be made:

1. The simulation results indicate that it is much easier to deal with geometric singularity by the RPIM for better accuracy, even for edge-cracked plate with a centric hole. As compared to analytical solution, the error obtained by RPIM is merely 1.15%, and -22.5% for the same case obtained by the FEM approach.

2. The simulation results for the temperature distribution of edge-cracked steel plate as subjected to lateral thermal loads on the right-hand side reveal that the edge-crack on the steel plate acting as an adiabatic barrier that prevents the heat on the right-hand side of the crack from passing through the gap, and thus enforce the heat to detour and retard the heat propagation leading to a longer conduction time.
3. The simulation results for the temperature distribution of the steel plate with a centric hole subject to T=100 °C on the upper boundary, T=500 °C around the centric hole, and T=50 °C on all other plate boundaries indicate that the temperature contours are somehow symmetric along horizontal x-direction, and become denser with higher temperature gradient in positive y-direction. Also, the displacements for nodes of higher temperature gradient are subject to tensile stress in positive y-direction, and for nodes of symmetric contour are subject to compressive stress along the horizontal x-direction. Thus, the temperature induced displacement phenomenon becomes distinct around centric hole areas.
4. For problems of irregular cracks and holes in the structure, the selection of proper locations and numbers of nodal points is crucial since that can significantly affect the modeling results, especially for problems with limited numbers of nodal points in numerical modeling process of RPIM.

## ACKNOWLEDGEMENT

The authors would like to thank the Ministry of Science and Technology for the supports under grant numbers MOST 106-2221-E-006-104.

## REFERENCES

- Atluri, S.N. and Zhu, T., "A New Meshless Local Petrov-Galerkin (MLPG) Approach," *Computational Mechanics*, Vol. 22, No. 2, pp. 117-127, 1998.
- Atluri, S.N. and Zhu, Y.T., "A Point Interpolation Method for Two-Dimensional Solids," *International Journal for Numerical Methods in Engineering*, Vol. 50, No. 4, pp. 937-951, 2001.
- Barta, J. "Über die Näherungsweise Lösung einiger Zweidimensionaler Elastizität Aufgaben," *J. Appl. Math. Mech.*, Vol. 17, No. 3, pp. 184-185, 1937.
- Belytschko, T., Lu, Y.Y. and Gu, L., "Element-free Galerkin Methods," *International Journal for Numerical Methods in Engineering*, Vol. 37, No. 2, pp. 229-256, 1994.
- Chorin, A.J., "Numerical Study of Slightly Viscous Flow," *Journal of Fluid Mechanics*, Vol. 57, pp. 785-796, 1973.
- Crank, J. and Nicolson, P.A., "Practical Method for Numerical Evaluation of Solutions of Partial Differential Equations of the Heat Conduction Type," *Proc. Camb. Phil. Soc.*, Vol. 43, No. 1, pp. 50-67, 1947.
- Gingold, R.A. and Monaghan, J.J., *Theory and*

- Application to Non-spherical Stars*, Oxford University Press, Oxford, U.K., pp. 375-389, 1977.
- Gingold, R.A. and Monaghan, J.J., *Smoothed Particle Hydrodynamics: Theory and Application to Non-spherical Stars*, Oxford University Press, Oxford, U.K., pp. 375-389, 1977.
- Gladwell, G.M.L., *Solid Mechanics and its Application*, Department of Civil Engineering, University of Waterloo, Waterloo, Ontario, Canada, 1996.
- Liu, G.R., Zhang, G.Y., Gu, Y.T., Wang, Y.Y., "A Meshfree Radial Point Interpolation Method (RPIM) for Three-dimensional Solids," *Computational Mechanics*, Vol. 36, No. 6, pp. 421-430, 2005.
- Lucy, L.B., "A Numerical Approach to the Testing of the Fission Hypothesis," *Astron. J.*, Vol. 82, pp. 1013-24, 1977.
- Nayroles, B., Touzot, G. and Villon P., "Generalizing the Finite Element Method: Diffuse Approximation and Diffuse Elements," *Computational Mechanics*, Vol. 10, pp. 307-318, 1992.
- Slater, J.C., "Electronic energy bands in metal," *Phys. Rev.*, Vol. 45, No. 11, pp. 794-801, 1934.
- Tanigawa, Y., "Some Basic Thermoelastic Problems for Nonhomogeneous Structural Materials," *Applied Mechanical Review*, Vol. 48, pp. 377-389, 1995.

## 波動負載與熱源環境下 具邊緣裂縫與中心孔平板 之熱彈和斷裂特性研究

賴新一 劉宣偉  
國立成功大學機械工程學系

### 摘要

本文探討邊緣裂縫與具中心孔之平板，在波動負載與環境受熱作用下的熱彈和斷裂特性。文中提出了一種徑向點內插無網格(RPIM)法，並將其應用於複雜問題的應力強度因子(SIF)估計上。結果表明，用 RPIM 得到的解比有限元得到的解更為精確。文中還詳細描述了邊緣裂紋位置和長度對承受波動負載和環境受熱平板位移的影響。模擬結果表明，採用本文所提出的 RPIM 法可以更有效、更準確地模擬出邊緣裂縫與具中心孔之平板的熱彈和斷裂之特性。